Supporting Information

Transparent, flexible $MAPbI_3$ perovskite microwire array passivated with ultra-hydrophobic supramolecular assembly for stable and high-performance photodetectors

K. D. M. Rao,[*‡a,b] Mozakkar Hossain, [‡a,b] Umesh,[a] Aniket Roy,[a] Anudeepa Ghosh,[c] Gundam Sandeep Kumar,[a] Parikshit Moitra,[a,b] Tapas Kamilya,[a] Somobrata Acharya,[*a] and Santanu Bhattacharya[*a,b,d]

[a] School of Applied & Interdisciplinary Sciences, Indian Association for the Cultivation of Science, Jadavpur, Kolkata 700032, India

[b] Technical Research Centre, Indian Association for the Cultivation of Science, Jadavpur, Kolkata 700032, India

[c] School of Physical Sciences, Indian Association for the Cultivation of Science, Jadavpur, Kolkata 700032, India

[d] Department of Organic Chemistry, Indian Institute of Science, Bangalore 560012, Karnataka, India

* E-mail: trckdmr@iacs.res.in, mallik2arjun@gmail.com (K. D. M. R.), sb23in@yahoo.com, sb@iisc.ac.in (S. B.), camsa2@iacs.res.in (S. A.).

‡ The authors equally contribute to this work.

Table of Contents

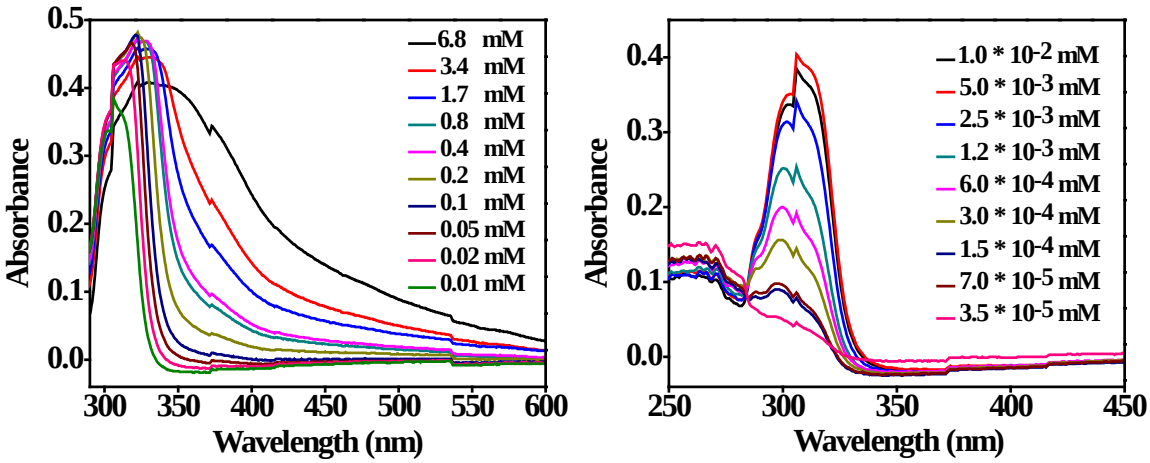

Figure S1: Concentration dependent UV-Visible spectra of Tripodal L-Phe-$C_{11}H_{23}$.

In order to investigate the self-assembly process, we performed UV-Visible spectroscopy by varying the concentration of the tripodal L-Phe-$C_{11}H_{23}$ molecule. From the concentration dependent UV-visible spectra a strong band at 340 nm appeared which is attributed to the π-π^* transition of aromatic rings present in the molecule. On decreasing the concentration, the UV-Vis band at 340 nm showed a blue shift indicating the existence of J-type of aggregates among the π-stacking moieties available in the self-assembled nanostructures generated by the tripodal L-Phe-$C_{11}H_{23}$. Although it is understood that the molecule, tripodal L-Phe-$C_{11}H_{23}$, is hydrophobic in nature on its own, we further added a fluorinated derivative, tripodal L-Phe-C_7F_{15}, into the tripodal L-Phe-$C_{11}H_{23}$ to enhance the hydrophobicity. The stoichiometry of tripod L-Phe-C_7F_{15} in tripod L-Phe-$C_{11}H_{23}$ was chosen to be 20% of molar ratio, which has optimal transparency and hydrophobicity (see table S2).

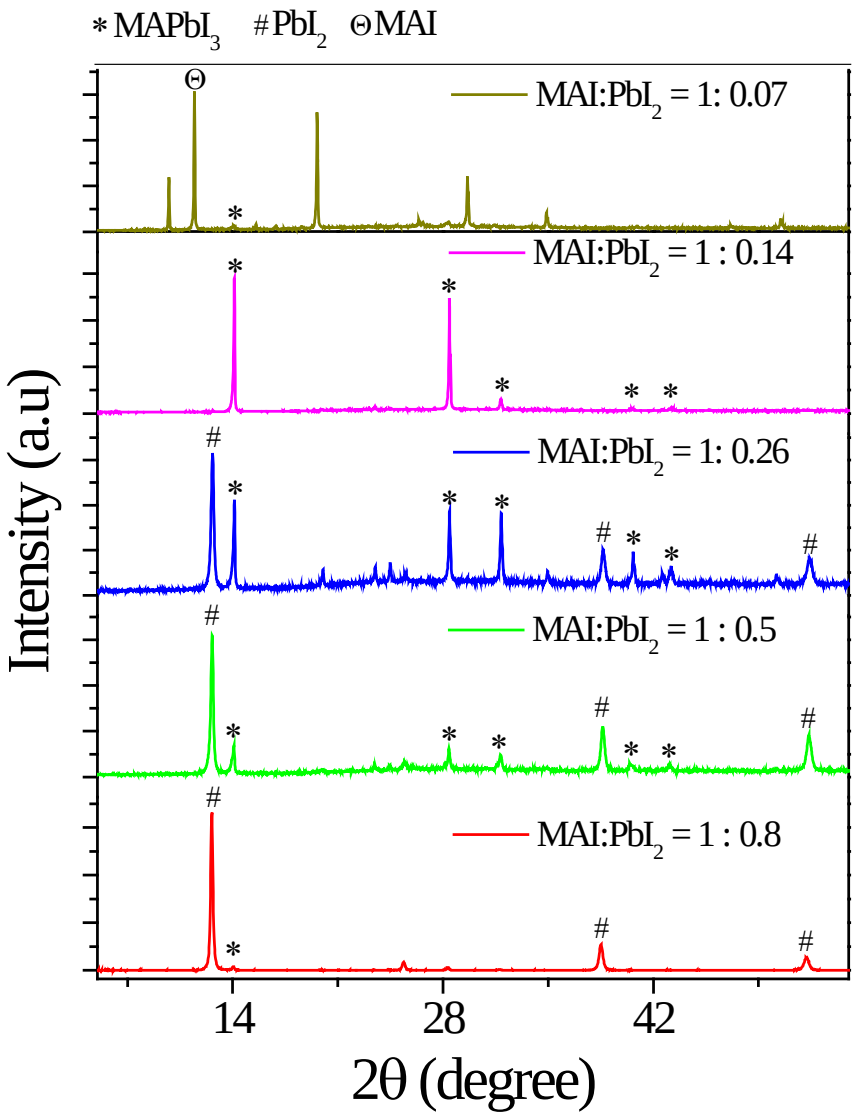

Figure S2: XRD patterns at different molar ratios of MAI and PbI_2.

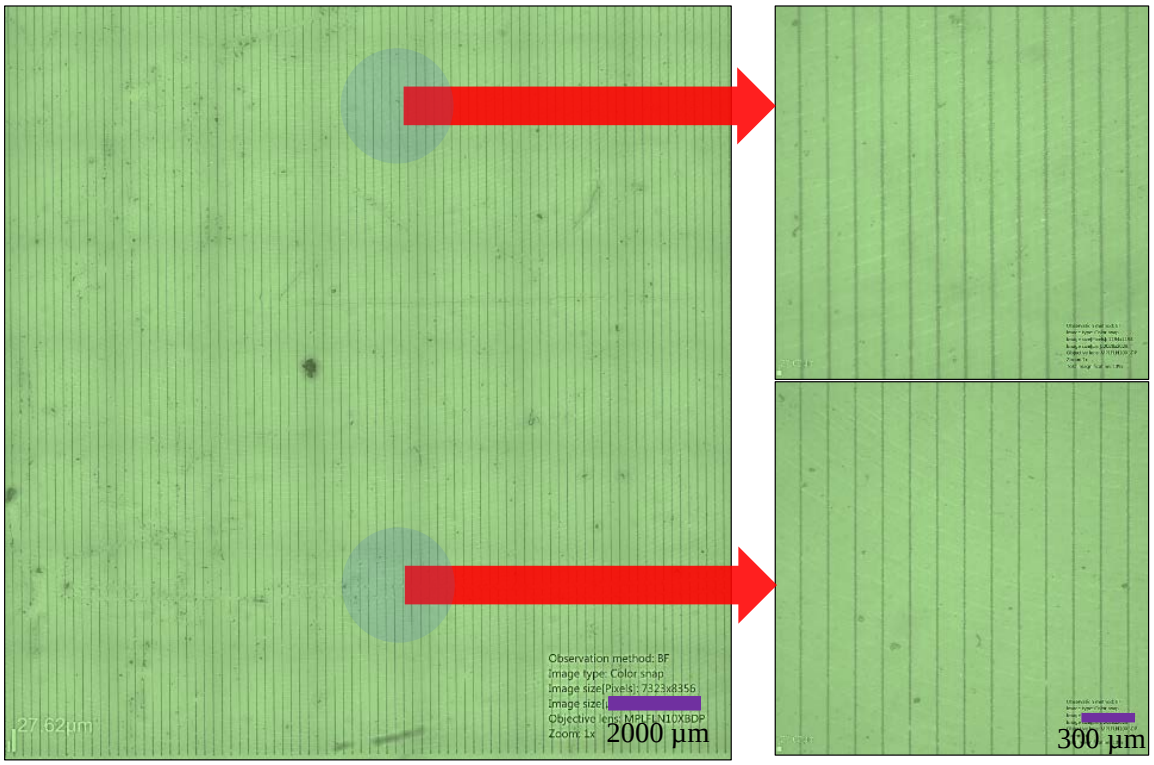

Figure S3. Optical microscope image of ultra-long $MAPbI_3$ MW array in 1.65 × 1.59 cm^2.

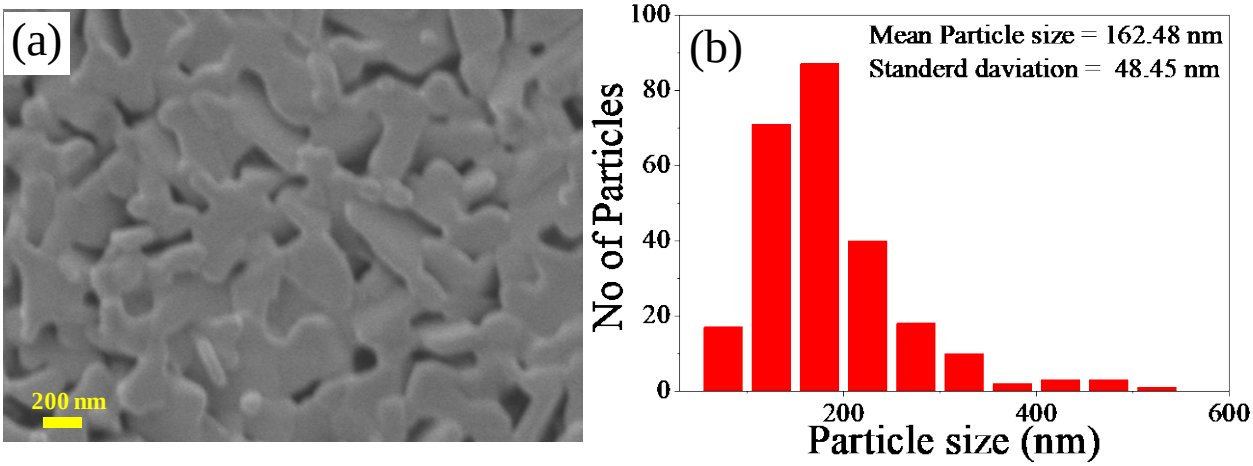

Figure S4. (a) FESEM image of single $MAPbI_3$ microwire at highest magnification. (b) Histogram of particle size distribution in $MAPbI_3$ microwire.

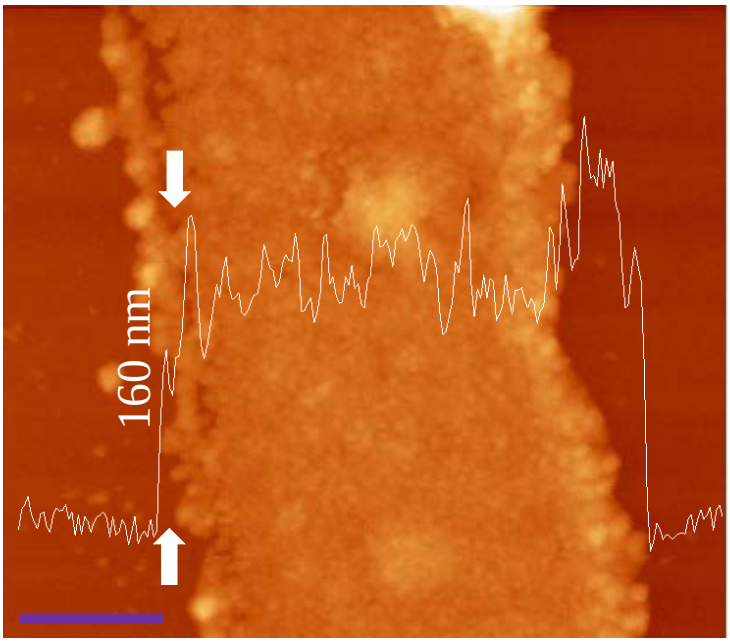

Figure S5. Atomic force microscopy image of single $MAPbI_3$ microwire (Scale Bar 4 µm).

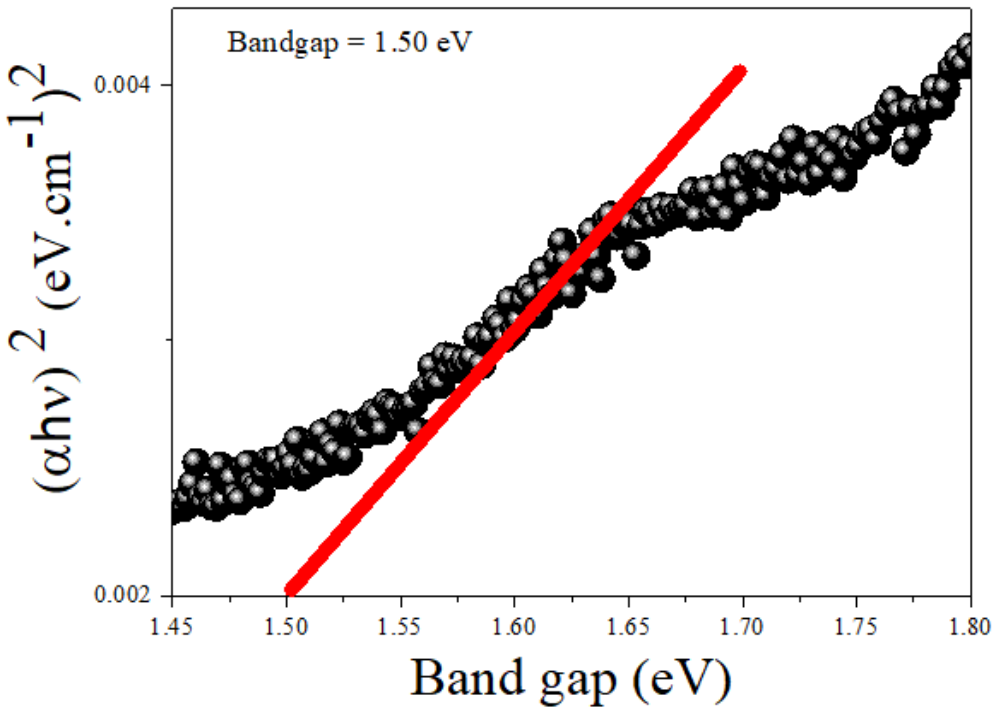

Figure S6. Band-gap estimation of ultra-long $MAPbI_3$ MW array from UV-Vis spectra.

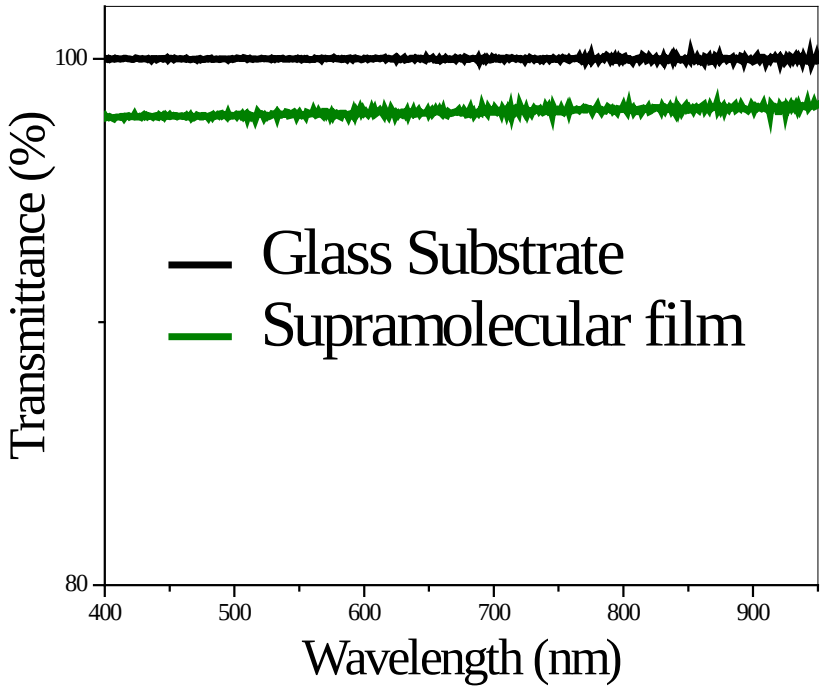

Figure S7. Transmittance spectra of Supramolecular thin film on the glass substrate.

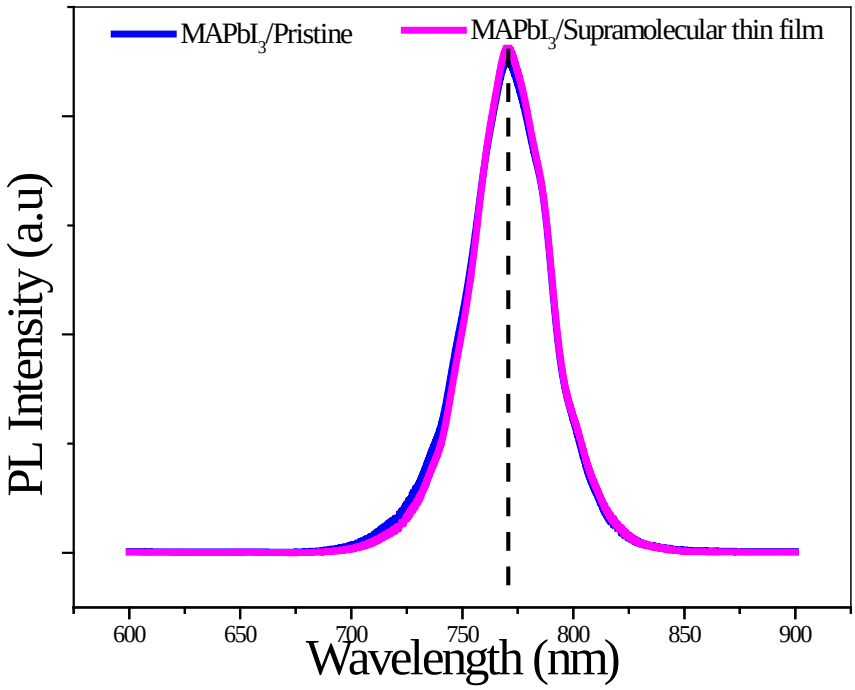

Figure S8. Photoluminescence spectra of pristine and supramolecular thin-film coated $MAPbI_3$ MW array.

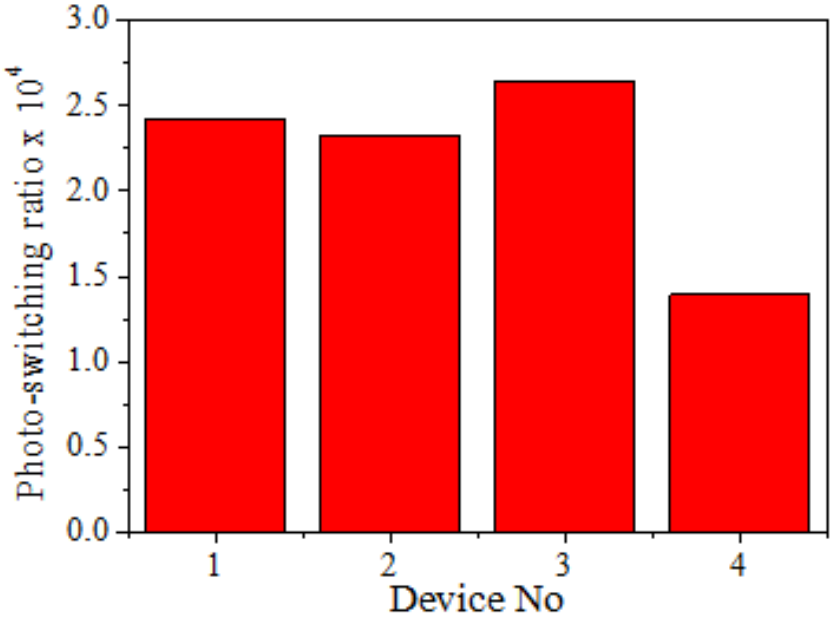

Figure S9. Statistics of photo-switching ratio for different photodetectors fabricated with ultra-long $MAPbI_3$ MW array.

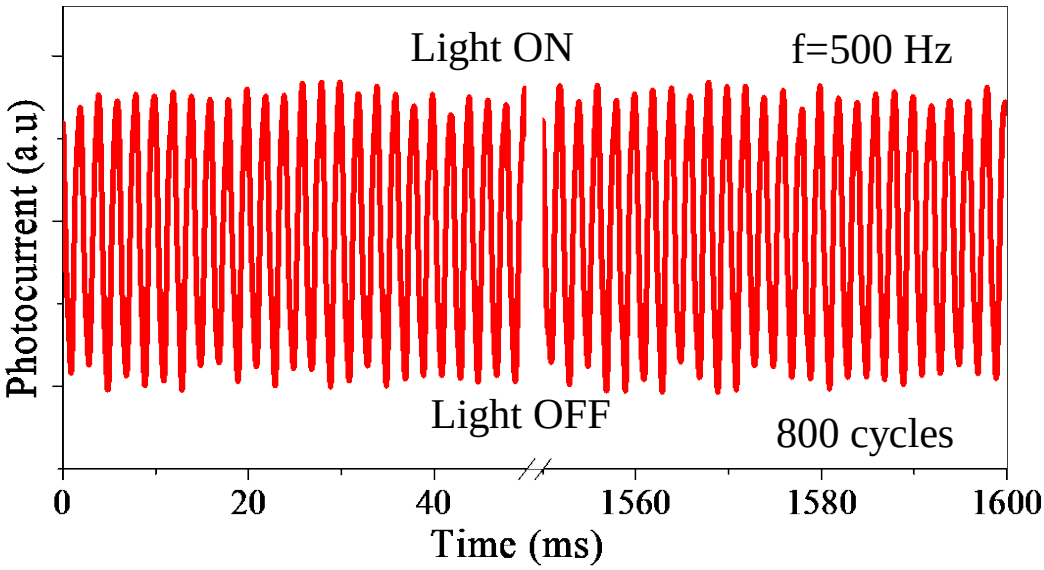

Figure S10. Photo-switching repeatability of ultra-long $MAPbI_3$ MW array based photodetector for 800 cycles at 5 V bias.

Section 1: Taut Plot

$$(\alpha h\upsilon)^{(\frac{1}{n})} = A(h\upsilon - E_g) \text{ ----------(S1)}$$

Where,

α = absorption coefficient (cm^{-1})

$h\upsilon$ = photon energy (eV)

n = ½ for direct bandgap semiconductor

A = constant

E_g= bandgap energy

Section 2: Linear Dynamic Range (LDR)

$$LDR = 20log\frac{J_{upper}}{J_{lower}} = 20log\frac{P_{upper}}{P_{lower}} \text{----------(S2)}$$

Where,

LDR = Linear Dynamic Range

J_{upper} = current density highest light intensity

J_{lower} = current density lowest light intensity

P_{upper} = highest light intensity

P_{lower} = lowest light intensity

Section 3: Responsivity (R_λ)

$$R_\lambda = \frac{J_{ph}}{P_{Light}} \text{----------(S3)}$$

$$J_{ph} = \frac{I_{ph}}{A} \text{----------(S4)}$$

Where,

R_λ= Responsivity

J_{ph}= photocurrent density

I_{ph}= I_l - I_d = photocurrent

I_l= light current

I_d= dark current

P_{Light}= light intensity

A = active area of the device

Section 4: Detectivity (D)

Detectivity can be estimated using the noise current as described by the following equation-S5. Detectivity is inversely proportional to the noise equivalent power (NEP), linearly proportional to the square root of electrical bandwidth and area of the device (A).

$D = \sqrt{A \times \Delta f}/NEP$..... (S5)

D = detectivity in cm $Hz^{1/2}$ W^{-1} or Jones

Δf = electrical bandwidth in Hz

A = device area in cm^2

NEP = noise equivalent power

The detector noise can limit the detectivity of the photodetector, which may have contributions from generation-recombination noise, shot noise, thermal noise, and 1/f noise. In the present scenario, shot noise from the dark current is dominant contribution. Therefore, NEP can be expressed as

$NEP = i_{n,s}/R_\lambda$..... (S6)

$i_{n,s}$ = shot noise current

R_λ = responsivity

Shot noise current can be approximated using the following equation

$i_{n,s} = \sqrt{2 \times q \times i_d \times \Delta f}$..... (S7)

q = charge of electron

i_d = dark current (nA)

Δf = electrical bandwidth in Hz

Replacing equation (S7), (S6) in equation (S5) we can end up having the simplified Detectivity equation as follows.

$D = R_\lambda/\sqrt{2 \times q \times J_d}$..... (S8)

J_d = dark current density in nA/cm^2.

Thus, it is evident that the dark current density (J_d) is originating from the shot noise current ($i_{n,s}$) present in the device. So, evaluating the detectivity using the above equation 4 containing dark current density (J_d) actually considers the shot noise current ($i_{n,s}$) of the device. The derivation of equation S8 from equation S5 is also well-established in the literature.[1]

Section 5: External Quantum Efficiency (EQE)

$$EQE = \frac{hcR_\lambda}{e\lambda} \text{----------(S9)}$$

Where,

EQE= External Quantum Efficiency

R_λ=responsivity

h = Planks Constant

c = Velocity of light in Vacuum

e = charge of electron

λ = wavelength of light

Section 6: Noise Equivalent Power (NEP)

$$NEP = S_I/R_\lambda \text{---------(S10)}$$

$$S_I = \sqrt{\frac{<I_{noise}{}^2>}{1\ Hz}} \text{--------(S11)}$$

Where,

NEP = Noise Equivalent Power

S_I = RMS dark noise spectral density (which corresponds to 1 Hz bandwidth).

I_{noise} = current in darkness

R_λ = wavelength responsivity

Section 7: Rise and fall time calculation

$$I = I_0 - I_0 \times e^{(-x/t_r)} \text{---------(S12)}$$

$$I = I_0 + A_1 \times e^{(-x/t_f)} \text{---------(S13)}$$

I = current

I_0 = initial value of current

A_1 = independent variables

t_r = rise time, t_f = fall time, x = time

Table S1: Literature comparison of Micro/nanostructured $MAPbI_3$ photodetectors

Ref No.	Micro/nano structured $MAPbI_3$	T[a)] %) at 550 nm	Flexibility	R[b)] (A/W)	D[c)] (Jones)	LDR[d)] (dB)	Response time
2	Network Array	~30	Yes,10000	0.10	$1.02x10^{12}$	------	0.3 ms
3	Nanoparticles	~60	Yes	$4.9x10^{-3}$	--	----	50 µs
4	Microwires	No	No	0.04	$0.6x10^{12}$	-----	178 µs
5	Thin Film	No	No	20.7	$6.5x10^{13}$	76	17 µs
6	Nanosheets	No	No	0.03	----	------	230 ms
7	Nanonets	No	Yes, 50	10.33	-----	-----	0.02 ms
8	Nanowires	No	Yes, 2000	410	$9.1x10^{12}$	-----	0.22 ms
9	Thin Film	No	No	----	$1.4x10^{12}$	73	23 µs
10	Nanowires	No	No	$55x10^{-3}$	$0.5x10^{11}$	-----	0.15s
11	Microwire Arrays	No	Yes,10^5	13.5	$5.2x10^{12}$	114	80 µs
12	Microwires	No	Yes, 5000	13.8	$3.8x10^{12}$	------	50 ms
13	Thin Films	No	No	----	----		40 ms
14	Nanoribbon Arrays	~65	Yes	0.04	$8.2x10^{11}$	-----	27 ms
15	Nano grating	Yes	No	58.5	----	-------	-----
16	Nanowires	No	Yes, 90	0.01	$3.5x10^{11}$	-----	12 ms
17	Nanowire	No	No	4.95	$2x10^{13}$	70	0.1 ms
Present work	Ultra-long $MAPbI_3$ MW array	~89	Yes, 1200	789	10^{14}	122	432/556 µs

[a)] Transmittance; [b)] Responsivity; [c)] Detectivity; [d)] Linear Dynamic Range

Table S2: Tripodal L-Phe-C_7F_{15} molecule doping in the Supramolecular self-assembly of Tripodal L-Phe-$C_{11}H_{23}$

Sl No.	Supramolecular self-assembly	Tripodal L-Phe-C_7F_{15} molecule (%)	Transmittance (%)	Contact Angle (Degree)
1	Tripodal L-Phe-$C_{11}H_{23}$	0	98.7	92.1
2	Tripodal L-Phe-$C_{11}H_{23}/C_7F_{15}$	10	98.2	102
3	**Tripodal L-Phe-$C_{11}H_{23}/C_7F_{15}$**	**20**	**98.2**	**105**
4	Tripodal L-Phe-$C_{11}H_{23}/C_7F_{15}$	50	96	105
5	Tripodal L-Phe-$C_{11}H_{23}/C_7F_{15}$	100	90	103.3

Section 8. Experimental Section

8.1 Synthesis of tripodal L-Phe-$C_{11}H_{23}$/-C_7F_{15} molecule for the Supramolecular Self-assembly:

Synthetic Scheme

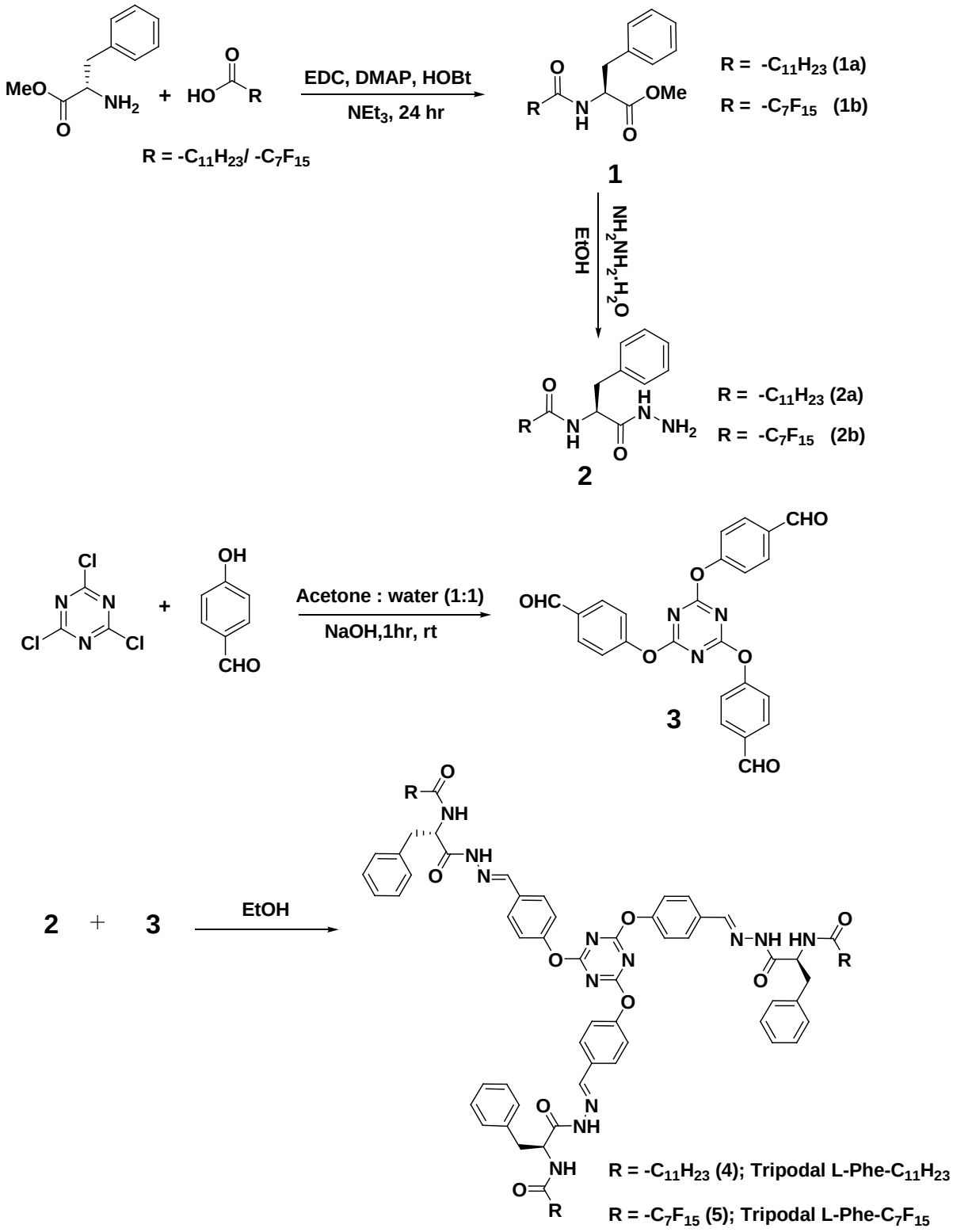

Synthetic Procedure:

Compound **1**, **2**, **3** and **4** were synthesized following the reported procedures.[18-20] The final compound **5** was synthesized as given below.

Synthesis of 5.

To a solution of **2b** (1 g, 2.7 mmol) in 30 mL of ethanol, **3** (1.2 g, 2.7 mmol) was added and the reaction mixture was refluxed for 12 hr. The reaction mixture was then evaporated under vacuum to yield a crude white powder which was further purified by silica column chromatography using 1% MeOH in $CHCl_3$ as eluent to give the pure desired product.

^{1}H-NMR ($CDCl_3$), δ (ppm): 7.76 (*s*, 3H), 7.30-6.94 (*m*, 5H), 5.86 (*d*, 3H), 4.91 (*m*, 3H), 3.17-3.08 (*m*, 6H).

^{13}C-NMR ($CDCl_3$), δ (ppm): 191.17, 164.34, 162.83, 157.48, 132.44, 130.78, 130.30, 129.49, 129.49, 129.42, 128.69, 128.45, 126.74, 121.26, 116.43, 49.29, 37.73, 33.94, 33.74, 29.65, 26.14, 25.89, 25.28, 24.99, 24.86.

FT-IR (cm^{-1}): 3325.80, 2928.20, 2857.04, 1670.82, 1566.52, 1508.8, 1449.85, 1366.57.

MALDI-MS: m/z calculated for (M^++K) 2168.1027; Observed 2167.9870.

8.2 Characterization of the Supramolecular Self-assembly:

^{1}H NMR studies were carried out on a Bruker DPX 400/500 MHz NMR spectrometer. Infrared (IR) spectra were recorded using a Perkin Elmer Spectrum BX FT-IR spectrometer. MALDI spectrum is recorded in Bruker MALDI-TOF New ultrafleXtreme spectrometer. Absorption spectra were taken using Shimadzu UV-2450 spectrophotometer after appropriate baseline correction. AFM imaging of the samples were performed with an Asylum Research MFP-3D AFM in tapping mode using AC160TS silicon probes, with nominal tip radii <10 nm. Energy minimisation of the molecules were calculated by B3LYP/6-31G* method using Gaussian-09 software.[21]

8.3 Fabrication ultra-long long $MAPbI_3$ MW arrays:

The initial precursors methylammonium iodide (MAI) (Luminescence Technology Corp.) and lead iodide (PbI_2) were purchased from Sigma-Aldrich and used as received. The metal stencils consist of continuous and repetitive linear apertures having holes of 13 µm width and length 2 cm with pitch 138 µm. These were purchased from Harshini Industries from Bangalore. Glass substrates were cleaned by washing in soap water, dipping in piranha solution (4:1, H_2SO_4:H_2O_2) for 20 minutes and followed by ultrasonication in Milli-Q water, acetone and isopropanol for 10 minutes each, respectively. The Glass/PET substrates were conformally attached with metal stencils and placed inside physical vapour deposition system (Hind High Vacuum Company Private Limited: model:12A4D). The precursors MAI and PbI_2 were placed in two different molybdenum boats in 1:0.14 molar ratio (MAI = 145 mg, PbI_2 = 58 mg) inside a vacuum chamber maintained at ~ (1-3) $\times 10^{-6}$ m. bar pressure. PbI_2 and MAI were evaporated sequentially (First PbI_2 followed by MAI) by controlling the current from 0 A to 33 A and maintaining the deposition rate below 5Å/s. The samples are annealed at 110° C for 30 minutes in N_2 atmosphere, after pulling out from the vacuum chamber. The supramolecular solution is prepared by mixing 18 mg tripodal L-phe-C_{11}-/-C_7F_{15} molecule in 1 ml toluene. The mixture is then dipped in hot water bath followed by ultrasonication for 2 min. The resultant supramolecular solution is spin-coated (Apex Instruments: SpinNXGP1) on top of the $MAPbI_3$ MW array with 1000 RPM for 60 sec.

8.4 Photodetector Device Fabrication

ITO gap electrodes on a glass substrate with a channel width of 20 µm and length of 2 mm are fabricated by photolithography followed by etching ITO in gap region. The ITO electrodes used for device fabrication demonstrated a transmittance of 90 %. The photocurrent and current-voltage characteristic measurements were performed with a TTPx Lakeshore probe station connected to a Keithley 4200/2634B semiconductor characterization system. The intensity of the white light source is modulated using light filters. For responsivity related measurements F&S Bondtech 40546AK5901 based wire bonder equipped with Leica S6 microscope is used to extract electrical connections from a single $MAPbI_3$ microwire fabricated over Au gap electrode with width 0.9 µm. The wavelength

dependent photocurrent measurements were performed using various LEDs different wavelengths. The bandwidth measurement was carried out by modulating white LED frequency from 10 Hz to 8 kHz using a function generator (Scientific Instruments, SM5070). While modulating LED light photoresponse of the $MAPbI_3$ photodetector is recorded with an oscilloscope (Scientific Instruments, SMO702). Long-term frequency domain measurements were carried out by modulating a red laser diode (LD-RL-6-5v, ~3 mW, 650 nm) with Thorlabs optical chopper (MC2000B-EC), and oscilloscope (Scientific Instruments, SMO702). For flexibility measurements, Al gap electrodes on PET substrate with channel width of 40 µm and channel length of 2 mm are using a shadow mask and physical vapour deposition. These devices are placed on curved surfaces having bending radii(r) 10 mm, 8 mm, 6 mm. Contact angle measurement system (Ossila Contact Angle Goniometer, L2004A1) was used to evaluate the hydrophobicity nature.

8.5 Characterization of $MAPbI_3$ MW array

$MAPbI_3$ MW arrays are characterized after depositing the materials on glass/PET substrate. XRD diffraction is performed in PAN analytical (X'Pert PRO, 40 kV, 30 mA, wavelength ~ 0.154 nm) and Bruker AXS D8 Advanced equipment (40 kV, 40 mA, wavelength ~ 0.15406 nm) with Cu Kα radiation. Optical microscope images are captured in Olympus microscope (CKX-41) and Leica DMi8 fluorescent microscope. Morphology of the $MAPbI_3$ wire and supramolecular is visualised using AFM (Vecco, di CP-II). Image of single $MAPbI_3$ wire-based device as well as interconnectivity of $MAPbI_3$ was visualized using FESEM (JEOL JSM-7500F). UV-vis absorbance/transmittance measurements are carried out by using Varian Cary 5000 UV-vis-NIR spectrophotometer. The transmittance measurements throughout this study are performed with respect to the glass/PET substrate. Photoluminescence (PL) spectra are collected by using the RAMAN spectrophotometer (Raman Triple spectrometer Jobin-Yvon T64000) by exciting the sample with Nd:YAG green laser (532.5 nm, ~ 10 µW power). PL mapping image is captured by using Leica DMi8 fluorescent microscope after exciting the material with 568 nm green laser.

REFERENCES

1. J. Miao and F. Zhang, *Laser Photonics Rev.*, 2019, **13**,1800204.
2. H. Deng, X. Yang, D. Dong, B. Li, D. Yang, S. Yuan, K. Qiao, Y.-B. Cheng, J. Tang and H. Song, *Nano Lett.*, 2015, **15**, 7963-7969.
3. Y. P. Jeon, S. J. Woo and T. W. Kim, *Appl. Surface Sci.*, 2018, **434**, 375-381.
4. S. Li, Y. Li, Z. Shi, L. Lei, H. Ji, D. Wu, T. Xu, X. Li and G. Du, *Sol. Energy Mater. Sol. Cells*, 2019, **191**, 275-282.
5. L. Ji, H.-Y. Hsu, J. C. Lee, A. J. Bard and E. T. Yu, *Nano Lett.*, 2018, **18**, 994-1000.
6. P. Li, B. N. Shivananju, Y. Zhang, S. Li and Q. Bao, *J. Phys. D: Appl. Phys.*, 2017, **50**, 094002.
7. W. Wang, Y. Ma and L. Qi, *Adv. Funct. Mater.*, 2017, **27**, 1603653.
8. Q. Zhou, J. G. Park, R. Nie, A. K. Thokchom, D. Ha, J. Pan, S. I. Seok and T. Kim, *ACS Nano*, 2018, **12**, 8406-8414.
9. X. Fu, N. Dong, G. Lian, S. Lv, T. Zhao, Q. Wang, D. Cui and C.-P. Wong, *Nano Lett.*, 2018, **18**, 1213-1220.
10. X. Zhang, C. Liu, G. Ren, S. Li, C. Bi, Q. Hao and H. Liu, *Nanomaterials*,2018, **8**, 318.
11. W. Deng, X. Zhang, L. Huang, X. Xu, L. Wang, J. Wang, Q. Shang, S.-T. Lee and J. Jie, *Adv. Mater*., 2016, **28**, 2201-2208.
12. Y. Chen, J. Zhang, J. Zhou, Y. Chu, B. Zhou, X. Wu and J. Huang, *Adv. Optical Mater.*, 2018, **6**, 1800469.
13. Y. Zhang, J. Du, X. Wu, G. Zhang, Y. Chu, D. Liu, Y. Zhao, Z. Liang and J. Huang, *ACS Appl. Mater. Interfaces*, 2015, **7**, 21634-21638.
14. S. Lim, M. Ha, Y. Lee and H. Ko, *Adv. Optical Mater.*, 2018, **6**, 1800615.
15. H. Wang, R. Haroldson, B. Balachandran, A. Zakhidov, S. Sohal, J. Y. Chan, A. Zakhidov and W. Hu, *ACS Nano*, 2016, **10**, 10921-10928.

16. D. Wu, H. Zhou, Z. Song, R. Liu and H. Wang, *J. Mater. Chem. C*, 2018, **6**, 8628-8637.

17. L. Gao, K. Zeng, J. Guo, C. Ge, J. Du, Y. Zhao, C. Chen, H. Deng, Y. He, H. Song, G. Niu and J. Tang, *Nano Lett.*, 2016, **16**, 7446-7454.

18. A. Pal, Y. K. Ghosh and S. Bhattacharya, *Tetrahedron*, 2007, **63**, 7334-7348.

19. R. Ongaratto, N. Conte, C. R. Montes D'Oca, R. C. Brinkerhoff, C. P. Ruas, M. A. Gelesky and M. G. Montes D'Oca, *New J. Chem.*, 2019, **43**, 295-303.

20. D. C. Tahmassebi and T. Sasaki, *J. Org. Chem.*, 1994, **59**, 679-681.

21. P. Moitra, K. Kumar, P. Kondaiah and S. Bhattacharya, *Angew. Chem. Int. Ed.*, 2014, **53**, 1113-1117.